Journal of Nuclear Medicine, published on June 11, 2015 as doi:10.2967/jnumed.115.156828

PET imaging of MMR-expressing macrophages in tumor stroma using ^{18}F-radiolabeled camelid single-domain antibody fragments.

Anneleen Blykers[1*], Steve Schoonooghe[2,3*], Catarina Xavier[1*], Kevin D'hoe[2,3], Damya Laoui[2,3], Matthias D'Huyvetter[1], Ilse Vaneycken[1,4], Frederik Cleeren[5], Guy Bormans[5], Johannes Heemskerk[1,4], Geert Raes[2,3], Patrick De Baetselier[2,3], Tony Lahoutte[1,4], Nick Devoogdt[1,2*], Jo A. Van Ginderachter[2,3*] and Vicky Caveliers[1,4*]

1 In vivo Cellular and Molecular Imaging laboratory (ICMI), Vrije Universiteit Brussel, Brussels, Belgium

2 Laboratory of Cellular and Molecular Immunology (CMIM), Vrije Universiteit Brussel, Brussels, Belgium

3 Laboratory of Myeloid Cell Immunology (MCI), VIB, Brussels, Belgium

4 Department of Nuclear Medicine, UZ Brussel, Brussels, Belgium

5 Laboratory for Radiopharmacy, KU Leuven, Leuven, Belgium.

*These authors contributed equally

Correspondence should be directed to Anneleen Blykers:

In vivo Cellular and Molecular Imaging (ICMI) laboratory, Vrije Universiteit Brussel, Laarbeeklaan 103, 1090 Brussels, Belgium. Tel: +32 2 477 4991; fax: +32 2 477 5017

E-mail address: anneleen.blykers@gmail.com

The authors have nothing to disclose.

Running title: Imaging of MMR+ TAMs using F-18 sdAb.

Word count: 4991 words

ABSTRACT

Tumor-associated macrophages (TAMs) constitute a major component of the stroma of solid tumors, encompassing distinct subpopulations with different characteristics and functions. We aim to identify M2-oriented tumor-supporting macrophages within the tumor microenvironment as indicators of cancer progression and prognosis, using PET imaging. This can be realized by designing Fluor-18 labeled camelid single-domain antibody fragments (sdAbs) specifically targeting the macrophage mannose receptor (MMR), which has been identified as an important biomarker on this cell population.

Methods: Cross-reactive anti-MMR sdAbs were generated after immunization of an alpaca with the extracellular domains of both human and mouse MMR. The lead binder was chosen based on comparisons of binding affinity and in vivo pharmacokinetics. The PET-tracer [^{18}F]FB-anti-MMR sdAb was developed using the prosthetic group N-succinimidyl-4-[^{18}F]fluorobenzoate ([^{18}F]-SFB), and its biodistribution, tumor targeting potential and specificity in terms of macrophage and MMR targeting was evaluated in mouse tumor models.

Results: Four sdAbs were selected after affinity screening but only 2 were found to be cross-reactive for human and mouse MMR. The lead anti-MMR 3.49 sdAb, bearing an affinity of 12 and 1.8 nM for mouse and human MMR; respectively, was chosen for its favorable in vivo biodistribution profile and tumor targeting capacity.

[^{18}F]FB-anti-MMR 3.49 sdAb was synthesized with a 5-10% radiochemical yield using an automated and optimized protocol. In vivo biodistribution analyses showed fast clearance via the kidneys next to retention in MMR-expressing organs and tumor. The kidney retention of the fluorinated sdAb was 20-fold lower compared to a ^{99m}Tc-labeled counterpart. Compared to MMR- and C-C chemokine receptor 2 (CCR2)-deficient mice, significantly higher uptake was observed in tumors grown in WT mice demonstrating the specificity of the ^{18}F-tracer for MMR and macrophages, respectively.

Conclusion: Anti-MMR 3.49 was denoted as the lead cross-reactive MMR-targeting sdAb. [^{18}F]-radiosynthesis was optimized, providing an optimal probe for PET imaging of the tumor-promoting macrophage subpopulation in the tumor stroma.

Key words: Macrophage Mannose Receptor (MMR), camelid single-domain antibody fragment (sdAb), fluorine-18, PET, tumor microenvironment.

INTRODUCTION

During tumor development, myeloid cells are attracted to the tumor stroma. These infiltrating immune cells are versatile, adopting different activation states in response to a changing microenvironment leading to subsets of tumor-associated macrophages (TAMs) with specialized functions (*1,2*). Two main morphologically distinct TAM subsets can be distinguished based on Major Histocompatibility Complex (MHC) class II expression levels in multiple mouse tumor models. Tumor-promotion has been linked with an accumulation of M2-oriented MHC II^{low} TAMs in lung and breast carcinoma (*3,4*). Accordingly, MHC II^{low} TAMs were found to reside primarily in less oxygenated zones, express hypoxia-regulated genes and facilitate the angiogenic switch (*5*). Interestingly, the Macrophage Mannose Receptor (MMR, CD206), a typical M2 cell surface marker, is upregulated on these tumor-promoting MHC II^{low} TAMs in all tumor models studied (*3-5*). It should be pointed out that the M1/M2 nomenclature has shortcomings and that a better positioning of TAM subsets within the spectrum of macrophage activation states is warranted (*6*).

Overall, it is becoming clear that a more detailed insight in the molecular and functional characteristics of the tumor stromal cells is crucial for a better understanding of cancer progression and response to treatment. This is also reflected in the fact that novel therapies are being developed aiming specifically at the stromal compartment or tumor-infiltrating immune cells. Together with these new therapies, targeted imaging probes are needed. The potential of radiolabeled camelid single-domain antibody fragments (sdAbs, VHH, Nanobodies®[1]) for imaging of macrophages and dendritic cells has been demonstrated (*7-9*). ^{99m}Tc-labeled sdAbs specifically targeting murine MMR were found to be interesting new probes for preclinical imaging of MHC II^{low} TAMs within the tumor microenvironment (*10*).

[1] Nanobody® is a trade name of Ablynx NV.

In order to validate anti-MMR sdAbs as imaging tools for ultimate clinical translation, new cross-reactive anti-mouse/human MMR sdAbs were generated. They enable clinical applications after preclinical validation in appropriate mouse models (*11*). ^{18}F is a very attractive PET-isotope with a 110 min half-life and low energy positron (maximally 0.635 MeV) emitted. In addition, an in-house cyclotron allows starting with high initial activities and distribution of ^{18}F-labelled compound between centers. Direct ^{18}F-fluorination methods of proteins are not suited as harsh reaction conditions such as high reaction temperatures and dipolar aprotic solvents are usually needed. Alternatively, radiofluorination can be achieved through the use of small ^{18}F-labeled reactive precursors that act as a "prosthetic tag" to the biomolecule (*12*). N-succinimidyl-4-[^{18}F]fluorobenzoate ([^{18}F]-SFB) is the most common prosthetic group used as synthon for protein labeling with ^{18}F (*12-14*).

Here, we describe the generation and selection of a lead cross-reactive anti-MMR sdAb, optimization of the ^{18}F-radiochemistry and validation of the PET-probe in mouse tumor models.

MATERIALS AND METHODS

sdAb Generation and Selection of Lead Compound

Anti-MMR sdAbs were isolated from an immune sdAb phage-display library after immunization of an alpaca (Vicugna pacos) according to a six-week alternating schedule of weekly injections of recombinant human (rhMMR) or mouse (rmMMR) monomeric fusion proteins (*11,15*). After production of sdAb-displaying bacteriophages in Escherichia Coli, biopannings and ELISA screenings were performed in order to select MMR binding sdAbs. Purification of the hexahistidine-tagged sdAbs from the periplasm was performed as described previously (*11,15*). The binding characteristics of selected sdAbs were compared using Surface Plasmon Resonance (SPR) and flow cytometry.

The detailed procedure is described in the supplemental materials and methods. BcII10, an irrelevant sdAb binding to a bacterial enzyme, was used as a nontargeting control nanobody (*16*). Anti-MMR sdAbs were radiolabeled using ^{99m}Tc tricarbonyl chemistry as previously described in order to compare the in vivo biodistribution profile and select a lead compound (*17-19*). In vitro specificity was established as described in the Supplemental data.

^{18}F Labeling of Lead sdAb

[^{18}F]-SFB-Synthesis. Cyclotron produced [^{18}F] fluoride was separated from ^{18}O enriched water on a SepPak™ light accell plus QMA anion exchange cartridge (Waters) and eluted using 600 µl of a solution containing 4.2 mg K_2CO_3 and 22.6 mg Cryptand (K_{222}) in acetonitrile/water (1:1) (ABX). The solvent was evaporated to generate the anhydrous K_{222}/K[^{18}F]F complex.

The [^{18}F]-SFB prosthetic group was synthesized using disposable cassettes (IFP™ nucleophilic) on a SynthERA® module (IBA Molecular) in a 3-step, one-pot reaction. A solution of 4 mg (0.011 mmol) ethyl 4-(trimethylammonium)benzoate (ABX) in 2 ml dimethylsulfoxide (DMSO) (Sigma-Aldrich) was added to the dried [^{18}F]F^--complex in the reaction vial and heated to 110 °C for 15 min to produce ethyl-4-[^{18}F]fluorobenzoate. This compound was hydrolysed at 95 °C for 5 min by adding 20 µl (0.02 mol) of a 0.1 M tetrapropylammoniumhydroxide (TPAOH) solution. Subsequent activation was carried out with 26 mg (0.072 mmol) of N,N,N',N'-tetramethyl-O-(N-succinimidyl)uronium hexafluorophosphate (HSTU) in 1ml acetonitrile (CH_3CN) at 110°C for 5 min to form N-succinimidyl 4-[^{18}F]fluorobenzoate ([^{18}F]-SFB). The reaction mixture was remotely transferred to a second Synthera®, diluted with 4 ml 4.8% acetic acid solution/8 ml 0.9% NaCl and purified on a solid phase extraction (SPE) cartridge. The cartridge was washed with 20 % aqueous CH_3CN (5 ml) and eluted with CH_3CN (2.5 ml). The purification was optimized using either a C18 plus short (Waters) or AFFINIMIP® (Polyintell) SPE

cartridge. The purified [^{18}F]-SFB was transferred to a conical vial, placed in a homemade semi-automatic module connected to the Synthera® box, and evaporated to dryness by means of gentle heating and nitrogen stream.

[^{18}F]FB-anti-MMR sdAb Synthesis . Conjugation conditions of the sdAb to [^{18}F]-SFB were optimized in terms of temperature, protein concentration, incubation time and pH. A solution of sdAb (50-250 µg, 3.7-18.5 nmol) in 300 µl borate buffer (0.1 M, pH 7.4-9.0) was prepared and added to the dried [^{18}F]-SFB (1.0-7.5 GBq) reaction vial. After incubation, the mixture was purified by size exclusion chromatography using a PD-10 column (GE Healthcare) and passed through a 0.22 µm filter (Millipore).

Radiochemical identity and purity were assessed by reversed-phase-HPLC using a Hitachi Chromaster system (VWR) connected to a diode array and γ-detector (Raytest). The identity of the main compound was confirmed using unlabeled sdAb as reference material. A polystyrene divinylbenzene copolymer column (PLRP-S 300 Å, 5 µm, 250/4 mm, Agilent) was used applying the following gradient (A: 0.1% TFA in water; B: 0.1% TFA in acetonitrile): 0-5 min 25% B; 5-7 min 25-34% B; 7-10 min 34-100% B; 10-25 min 100% B at a flow rate of 1 ml min^{-1} (t_R [^{18}F]FB-anti-MMR sdAb = 12.5 min, [^{18}F]$^-$= 3-4 min; [^{18}F]-SFB = 13.5 min).

Animal Models

Wild type (WT) C57BL/6 mice (Janvier) were used for in vivo stability studies. To evaluate biodistribution and targeting specificity, C57BL/6 WT, MMR-deficient (MMR-KO) and C-C Chemokine receptor type 2-deficient (CCR2-KO) mice were subcutaneously inoculated in the right flank with 3x10^6 of the 3LL-R clone of Lewis Lung carcinoma cells suspended in HBSS-medium. Tumors were allowed to grow for 12 days (750-1000 mm^3). The local ethics committee for animal research has approved the study protocol.

Biodistribution Studies and PET/CT Imaging

3LL-R tumor-bearing mice, anesthetized with 2.5% isoflurane, were injected intravenously with ^{99m}Tc-anti-MMR sdAb (30-70 MBq, 5 µg sdAb) or [^{18}F]FB-anti-MMR sdAb (3.2-4.0 MBq, 5 µg sdAb) via the tail vein. Mice were sacrificed at 3 h post-injection, major organs collected, weighed and counted against a standard of known activity in a gamma counter. Tissue/organ uptake was calculated and expressed as a percentage of the injected activity per gram (%IA/g), corrected for decay. From a separate group of animals blood samples were collected 1, 5, 10, 20, 40, 60 and 120 minutes after [^{18}F]FB-anti-MMR sdAb injection, via a microcapillary, and analyzed in the gamma counter to obtain a blood time-activity curve. The half-life was calculated using a bi-exponential nonlinear regression fit (GraphPad Prism). Furthermore, urine samples of 3 mice were collected after 30 minutes and injected on RP-HPLC to detect radiometabolites.

Small animal PET was performed on a Focus™ 220 microPET scanner (Concorde Microsystems). Mice were injected with 8.8-9.3 MBq of the tracer via the tail vein and after 60 and 180 minutes, static PET-scans were acquired together with microCT scans to provide anatomical information and attenuation correction of the PET-signal. During all scanning sessions, animals were kept under gas anesthesia (2.5% isoflurane). High-resolution images were reconstructed using filtered back-projection (FBP) and maximum a posteriori (MAP) for microPET and microCT respectively. Image viewing was performed with AMIDE imaging software. Regions of interest (ROI) were drawn over the tumor to evaluate tracer accumulation.

Autoradiography

Dissected tumors were freshly frozen using O.C.T.-solution (VWR). Tumor sections (5-10 µm) were obtained using a cryotome (Shandon cryotome FSE; Thermo Fisher), mounted on adhesive microscope slides (Superfrost Plus; Thermo Fisher) and exposed to a phosphor storage screen film (Perkin Elmer) for about 12 h. The screens were read

using a Cyclone Plus system (Perkin Elmer) and analysed using Optiquant software (Perkin Elmer).

Statistical Analysis

Quantitative data are expressed as mean ± standard deviation (SD) and compared using the independent t-test after proving normal distribution via the Shapiro-Wilk test using SPSS Statistics.

RESULTS

Anti-human/mouse MMR sdAb Generation and Selection of a Lead Compound

sdAbs were generated against the recombinant extracellular domains of human and mouse MMR. ELISA screenings and sequencing of individual clones led to the identification of 27 clonally unrelated sdAb families. From these, 17 families appeared to be cross-reactive with hMMR and mMMR. SPR measurements of 30 different sdAbs, out of these families, revealed several binders with nanomolar affinity. Based on the observed affinities and diversity in CDR3 regions, four potentially cross-reactive clones (14.4, 5.38, 26.7 and 3.49; Table 1) were selected for a more in depth in vitro characterization. Among them, only 14.4 and 3.49 showed affinity for both human and mouse MMR-expressing cells in flow cytometry (Figure 1), suggesting that only these Nbs recognize both the recombinant and native versions of MMR. Subsequently, anti-MMR 3.49 and 14.4 were labeled with ^{99m}Tc and a biodistribution study in 3LL-R tumor-bearing showed fast renal clearance in addition to specific retention in liver, spleen, lymph nodes, bone and tumor (Table 2). Superior features in comparison with ^{99m}Tc-anti-MMR 14.4, including higher tumor and lower spleen and liver uptake, designated anti-MMR 3.49 sdAb as the lead compound. Binding specificity of ^{99m}Tc-anti-MMR 3.49 was assessed by an in vitro blocking study on recombinant MMR (Supplemental Figure 1) and importantly, target specificity was also confirmed in vivo as no tracer uptake was

observed in MMR-deficient mice, except for the normal excretion route (Table 2).

^{18}F Labeling of the Lead sdAb

Radiofluorination of anti-MMR 3.49 sdAb was accomplished by conjugation of the antibody fragment to the prosthetic group [^{18}F]-SFB. [^{18}F]-SFB was synthesized on a SynthERA® module in a 3-step, one-pot reaction. Synthesis and purification resulted in a radiochemical yield of 50-60 % in 90 minutes with a radiochemical purity >95 %. For subsequent conjugation, addition of 1 mg/ml sdAb in 0.1 M borate buffer pH 8.4-8.5 and incubation for 20 min at room temperature, resulted in the generation of [^{18}F]FB-anti-MMR 3.49 with a 20-30 % decay-corrected conjugation yield. A pH below 8.5 (pH 7.4-8.3) lowered the reactivity of the sdAbs' amino groups towards acylation, while a pH above 8.5 (pH 8.6-9.0) induced degradation of [^{18}F]-SFB, decreasing the coupling yield in both cases to 5-15 % (decay corrected) as shown in Supplemental Table 1. This accelerated [^{18}F]-SFB-degradation was also observed after longer reaction times. A radiochemical purity >97 % (Figure 2) and a global yield of 5-15 % (decay corrected, starting from [^{18}F]F^-) in 180 minutes were obtained. Furthermore, the tracer was stable in PBS pH 7.4 for at least 3 hours (Figure 2). The specific activity (SA) ranged from 10 to 30 GBq/µmol.

In vivo Biodistribution and Tumor Targeting of [^{18}F]FB-anti-MMR sdAb

[^{18}F]FB-anti-MMR 3.49 injection in 3LL-R tumor-bearing mice showed specific retention in MMR-expressing organs/tissues, including tumor (2.40 $\pm$ 0.46 % IA/g), while negligible uptake was observed in MMR-deficient hosts (Table 3). Importantly, tumor uptake of the tracer in CCR2-deficient mice, which contain strongly reduced macrophage numbers in the tumor microenvironment, was significantly lower ($p<0.05$) than the tumor uptake in WT mice (Table 3) confirming the in vivo recognition of tumor-associated macrophages. The low bone uptake indicated that no in vivo defluorination occurred. Remarkably, kidney uptake of ^{18}F-sdAb 3 h after tracer injection (Table 3) was about 20-fold lower as compared to the ^{99m}Tc-labeled sdAb in the same tumor model (Table 2). Furthermore, a significant decrease in extratumoral uptake in liver and spleen was also observed (Figure 3).

The blood time-activity curve confirmed rapid clearance of ^{18}F-sdAb from the blood, following a biphasic profile (Supplemental Figure 2) with half-lives of 1.4 min and 39.1 min. RP-HPLC analysis of urine samples obtained from naive mice injected with [^{18}F]FB-anti-MMR 3.49 sdAb confirmed metabolisation (Figure 2), which enhanced the elimination of activity from the kidneys.

PET images were in line with the ex vivo biodistribution data. The highest signal was present in the bladder, confirming renal clearance. Furthermore, specific retention in the tumor (Figure 4) and MMR-expressing tissue such as the liver (Supplemental Figure 3) was observed. In MMR-deficient mice the tracer was excreted without uptake in tissues or organs except for kidneys and bladder, strengthening the target specificity of the tracer. A 3 times higher mean uptake in tumor grown in WT-mice compared to tumors grown in MMR-deficient mice was measured. Intratumoral tracer distribution, using ex vivo autoradiography (Figure 4), showed a non-homogeneous pattern, with higher uptake at the border and some focal hotspots.

DISCUSSION

Immune cells, and especially macrophages, present in the tumor stroma contribute to cancer development (*1-4*). The MMR receptor (CD206) was identified as a marker for M2-oriented MHC II^{low} TAM, which were shown to be strongly angiogenic and immunosuppressive, suggestive of a tumor-promoting role in vivo (*3*). Accordingly, the presence of M2-oriented macrophages significantly correlates with a worse prognosis in multiple tumor types (*20,21*). Moreover, MHC II^{low} TAMs are predominantly present in hypoxic zones of the tumor stroma, albeit that the lower oxygen tension is not the major driver of the polarization into a MHC II^{low} MMR^{hi} phenotype (*5*). This suggests a scenario in which macrophages are skewed towards a MHC II^{hi}/MMR^{low} or a MHC II^{low}/MMR^{hi} phenotype under the influence of microenvironmental cues other than hypoxia, with the latter population preferentially migrating to hypoxic tumor areas. Given this knowledge, non-invasive imaging of MMR^{hi} TAM could be of prognostic value and might aid in the visualization of hypoxic tumor areas.

Single domain antibody fragments (10-15kDa) can be used for molecular imaging following their efficient tumor penetration in combination with rapid tracer elimination from circulation, enabling imaging at early time points. MMR-specific cross-reactive sdAbs that recognize both the mouse and human target biomarker were generated to trace MMR^{hi} cells in animal tumor models with a clear prospect towards clinical translation (*22*). The path from sdAbs generation after alpaca immunization to the selection of a lead candidate for MMR imaging involved a number of affinity screening assays and has identified anti-MMR 3.49 sdAb for the development of ^{18}F-radiochemistry and further in vivo characterization. Compared to SPECT, PET may improve the imaging of the tumor stroma because of its inherently higher sensitivity and substantially better and more uniform spatial resolution. The synthesis of [^{18}F]-SFB was successfully automated on SynthERA® following a 3-step, one-pot synthesis. In

comparison with Ackermann et al. (*23*), our optimized synthesis protocol required a larger reaction volume for fluorination and no drying step after basic hydrolysis. The use of more than 4 mg precursor resulted in more impurities with minor increase of labeling yield. As such, after optimization of the reaction steps, a reliable synthesis was obtained in 50 minutes with a 60-70% decay corrected yield. Instead of using 3 purification cartridges, one cartridge was sufficient to remove impurities as reported by Thonon et al (*13*). A conventional C18-cartridge was compared with a molecularly imprinted cartridge. Although the chemical purity was higher using AFFINIMIP® (no excess of precursor identified using mass spectrometry, data not shown) radiochemical purity after C18 purification stayed above 95%, enabling the use of both.

Comparable or lower conjugation yields are described when coupling [^{18}F]-SFB to diabodies resulting in conjugation yields of 5 to 15% (*24,25*). Nevertheless, dissolving [^{18}F]-SFB in organic solvent omitted its low stability in aqueous conditions and improved conjugation yields (*26-29*). Moreover, these conjugation yields exceeding 20% are only achievable when highly concentrated protein or peptide solutions are provided, in agreement with the conclusion of Wuest et al. (*30*). 1 mg/ml sdAb solution, in our case, provided acceptable yields exceeding 20 %. The automated protocol enabled the production of [^{18}F]FB-anti-MMR sdAb with sufficient activity to perform a clinical study (200-500 MBq).

[^{18}F]FB-anti-MMR sdAb specifically recognized MMR in 3LL-R bearing mice when compared with tracer uptake in the MMR-deficient tumor-recipients and was rapidly cleared from the circulation, as evidenced by both small animal PET imaging and biodistribution studies. In addition, CCR2-deficient mice were used to assess the recognition of macrophages. These mice have strongly reduced monocyte numbers in their circulation, leading to much lower levels of monocyte-derived macrophages in inflammatory sites such as tumors, including 3LL-R tumors (*3*). Decreased tumor uptake

in CCR2-deficient animals supports targeting of stromal macrophages.

Importantly, the degree of kidney retention of fluorinated sdAb is 20-fold lower compared to its ^{99m}Tc-analog at the 3h time point. Renal catabolism probably produced hydrophobic or non-residualizing metabolites, which diffuse out of the tubular cells and are in this way more easily cleared from the body (*31,32*). This hypothesis was supported by the identification of radiometabolites in urine. In contrast, radiometal labeled counterparts have the tendency to be retained in kidneys (*32*). Moreover, the fluorinated tracer showed decreased binding to extratumoral sites, while preserving tumor targeting. Although speculative, this could be attributed to distinct physiological properties of ^{99m}Tc and ^{18}F-labeled probes: different specific activities, charge, processing of the probe after receptor binding in liver and spleen (the MMR-positive organs that are mostly affected by the differential labeling strategies) and metabolization (*25*). The different specific activities of the radiolabeled sdAbs results in various ratios of labeled/non-labeled sdAb injected, the latter could contribute to binding to and blocking available receptors depending on blood flow and vascular permeability in the concerning tissue.

The preclinical in vivo results show high potential for clinical implementation as the combination of the fluorine-18 label (PET), with the specificity and affinity of camelid single-domain antibody fragments is promising. Because the presence of MMR^{hi} M2-like TAMs correlates with malignant progression, this probe could have significant added value in staging solid tumors and as a prognostic tool.

CONCLUSION

Cross-reactive anti-MMR sdAbs were produced and screened. Anti-MMR 3.49 sdAb was selected as the most potent candidate for the development of a new PET radiopharmaceutical. An efficient and reproducible ^{18}F-labeling approach was developed and the biological behavior of the tracer towards macrophage and MMR targeting was investigated. [^{18}F]FB-anti-MMR sdAb is a favorable new PET probe for detecting MMR-expressing tumor-associated macrophages, providing prognostic information about the tumor stroma.

DISCLOSURE

The authors have nothing to disclose.

ACKNOWLEDGMENTS

The authors thank Ludo De Vis, Cindy Peleman, Julie Cornelis and Andrey Postnov for technical assistance. Onderzoeksproject gerealiseerd met de steun van de Vlaamse Liga tegen Kanker - Stichting van Openbaar Nut. This work was funded by Nationaal Kankerplan Actie 29, Scientific Fund W. Gepts UZ Brussel and IWT-SBO Inflammatrack.

REFERENCES

1. Lewis CE, Pollard JW. Distinct role of macrophages in different tumor microenvironments. *Cancer Res.* 2006;66:605–612.

2. Allavena P, Sica A, Solinas G, Chiara Porta C, Mantovani A. The inflammatory microenvironment in tumor progression: the role of tumor-associated macrophages. *Crit Rev Oncol Hematol.* 2008;66:1–9.

3. Movahedi K, Laoui D, Gysemans C et al. Different tumor microenvironments contain functionally distinct subsets of macrophages derived from Ly6C(high) Monocytes. *Cancer Res.* 2010;70:5728-5739.

4. Laoui D, Van Overmeire E, Movahedi K et al. Mononuclear phagocyte heterogeneity in cancer: different subsets and activation states reaching out at the tumor site. *Immunobiology.* 2011;216:1192-1202.

5. Laoui D, Van Overmeire E, Di Conza G et al. Tumor hypoxia does not drive differentiation of tumor-associated macrophages but rather fine-tunes the M2-like macrophage population. *Cancer Res.* 2014;74:24-30.

6. Murray PJ, Allen JE, Biswas SK et al. Macrophage activation and polarization: nomenclature and experimental guidelines. *Immunity*. 2014;41:14-20.

7. Hamers-Casterman C, Atarhouch T, Muyldermans S et al. Naturally-occurring antibodies devoid of light-chains. *Nature.* 1993;363:446-448.

8. Schoonooghe S, Laoui D, Van Ginderachter JA et al. Novel applications of nanobodies for in vivo bio-imaging of inflamed tissue in inflammatory disease and cancer. *Immunobiology*. 2012;217:1266-1272.

9. De Groeve K, Deschacht N, De Koninck C et al. Nanobodies as tools for in vivo imaging of specific immune cell types. *J Nucl Med*. 2010;51:782-789.

10. Movahedi K, Schoonooghe S, Laoui D et al. Nanobody-based targeting of the macrophage mannose receptor for effective in vivo imaging of tumor-associated macrophages. *Cancer Res*. 2012;72:4165-4177.

11. Broisat A, Hernot S, Toczek J et al. Nanobodies targeting mouse/human VCAM1 for the nuclear imaging of atherosclerotic lesions. *Circ Res*. 2012;110:927-937.

12. Miller PW, Long NJ, Vilar R, Gee AD. Synthesis of ^{11}C, ^{18}F, ^{15}O, and ^{13}N radiolabels for positron emission tomography. *Angew Chem Int Ed Engl*. 2008;47:8998-9033.

13. Thonon D, Goblet D, Goukens E et al. Fully automated preparation and conjugation of N-succinimidyl 4-[^{18}F]fluorobenzoate ([^{18}F]SFB) with RGD peptide using a GE FASTlab™ synthesizer. *Mol Imaging Biol*. 2011;13:1088-1095.

14. Tang G, Zeng W, Yu M, Kabalka G. Facile synthesis of N-succinimidyl 4-[^{18}F]fluorobenzoate ([^{18}F]SFB) for protein labeling. *J Label Compd Radiopharm*. 2008;51:68-71.

15. Vincke C, Gutiérrez C, Wernery U, Devoogdt N, Hassanzadeh-Ghassabeh G, Muyldermans S. Generation of single domain antibody fragments derived from camelids and generation of manifold constructs. *Methods Mol Biol*. 2012;907:145-176.

16. Conrath KE, Lauwereys M, Galleni M et al. Beta-lactamase inhibitors derived from single-domain antibody fragments elicited in the camelidae. *Antimicrob Agents Chemother*. 2001;45:2807-2812

17. Vaneycken I, Devoogdt N, Van Gassen N et al. Preclinical screening of anti-HER2 nanobodies for molecular imaging of breast cancer. *Faseb J*. 2011;25:2433-2446.

18. Tchouate Gainkam LO, Huang L, Caveliers V et al. Comparison of the biodistribution and tumor targeting of two ^{99m}Tc-labeled anti-EGFR nanobodies in mice, using pinhole SPECT/micro-CT. *J Nucl Med*. 2008;49:788-795.

19. Xavier C, Devoogdt N, Hernot S et al. Site-specific labeling of his-tagged nanobodies with ^{99m}Tc: a practical guide. *Methods Mol Biol.* 2012;911:485-490.

20. Galon J, Costes A, Sanchez-Cabo F et al. Type, density, and location of immune cells within human colorectal tumors predict clinical outcome. *Science.* 2006;313:1960–1964.

21. Qian BZ, Pollard JW. Macrophage diversity enhances tumor progression and metastasis. *Cell.* 2010;141:39–51.

22. De Vos J, Devoogdt N, Lahoutte T, Muyldermans S. Camelid single-domain antibody-fragment engineering for (pre)clinical in vivo molecular imaging applications: adjusting the bullet to its target. *Expert Opin Biol Ther*. 2013;13:1149-60.

23. Ackermann U, Yeoh SD, Sachinidis JI, Poniger SS, Scott AM, Tochon-Danguy HJ. A simplified protocol for the automated production of succinimidyl 4-[F-18] fluorobenzoate on an IBA Synthera module. *J Label Compd Radiopharm.* 2011;54;671-673.

24. Olafsen T, Sirk SJ, Olma S, Shen CKF, Wu AM. ImmunoPET using engineered antibody fragments: fluorine-18 labeled diabodies for same-day imaging. *Tumor Biol*. 2012;33:669–677.

25. Cai W, Olafsen T, Zhang X, Cao Q, Gambhir SS, Williams LE, Wu AM, Chen X. PET imaging of colorectal cancer in xenograft-bearing mice by use of an ^{18}F-labeled T84.66 anti-carcinoembryonic antigen diabody. *J Nucl Med.* 2007;48:304-310.

26. Di Gialleonardo V, Signore A, Glaudemans AWJM, Dierckx RAJO, De Vries EFJ. N-(4-^{18}F-fluorobenzoyl)interleukin-2 for PET of human-activated T lymphocytes. *J Nucl Med.* 2012;53:679-686.

27. Lapi SE, Wahnishe H, Pham D et al. Assessment of an ^{18}F-labeled phosphoramidate peptidomimetic as a new prostate-specific membrane antigen–targeted imaging agent for prostate cancer. *J Nucl Med.* 2009;50:2042-2048.

28. Zhang X, Cai W, Cao F et al. ^{18}F-labeled bombesin analogs for targeting GRP receptor-expressing prostate cancer. *J Nucl Med*. 2006;47:492-501.

29. Johnström P, Clark JC, Pickard JD, Davenport AP. Automated synthesis of the generic peptide labelling agent N-succinimidyl 4-[^{18}F]fluorobenzoate and application to ^{18}F-label the vasoactive transmitter urotensin-II as a ligand for positron emission tomography. *Nucl Med Biol*. 2008;35:725-731.

30. Wuest F, Köhler L, Berndt M, Pietzsch J. Systematic comparison of two novel, thiol-reactive groups for ^{18}F-labeling of peptide and proteins with the acylating agent N-succinimidyl-4-[^{18}F]-fluorobenzoate ([^{18}F]-SFB). *Amino Acids*. 2009;36:283–295.

31. Rosik D, Thibblin A, Antoni G et al. Incorporation of a triglutamyl spacer improves the biodistribution of synthetic affibody molecules radiofluorinated at the N-Terminus via oxime formation with ^{18}F-4-Fluorobenzaldehyde. *Bioconjug Chem*. 2014;25:82-92.

32. Wu AM. Engineered antibodies for molecular imaging of cancer. *Methods.* 2014; 65: 139-147.

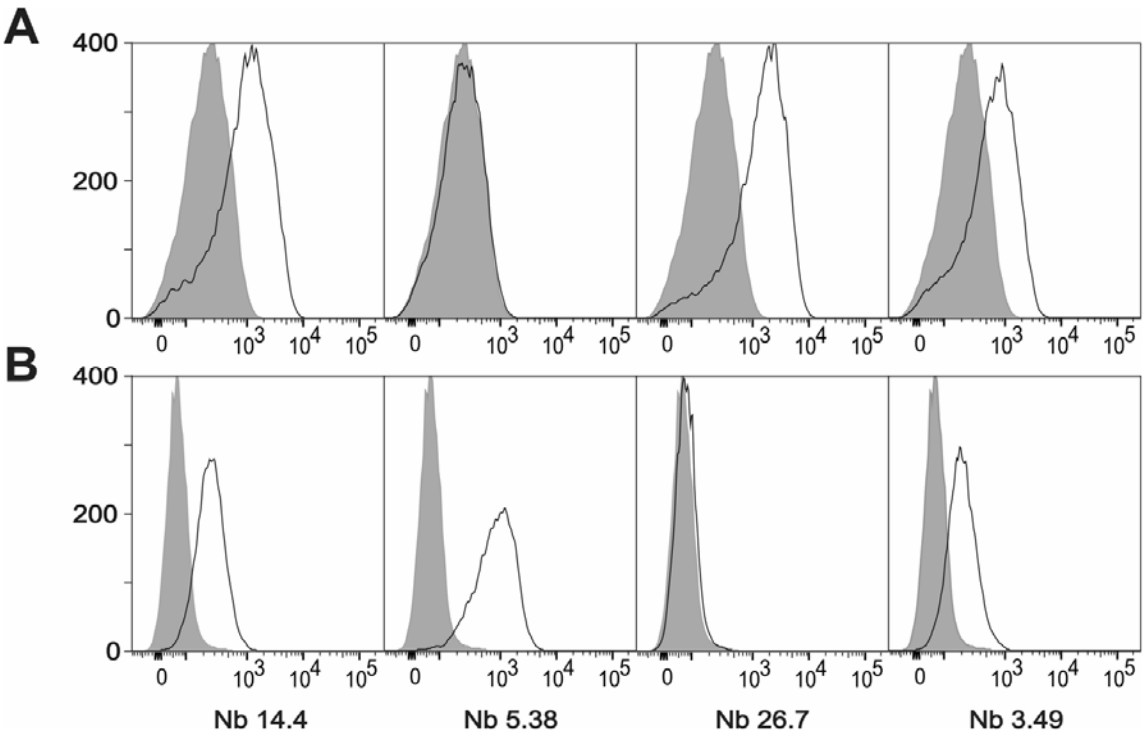

Figure 1: A. Staining of single cell suspensions prepared from 15 day old 3LL-R subcutaneous tumors grown in C57Bl/6 WT mice. B. Staining on immature human dendritic cells (iDC's) expressing hMMR. Shaded histograms represent sdAb BCII10 negative control staining.

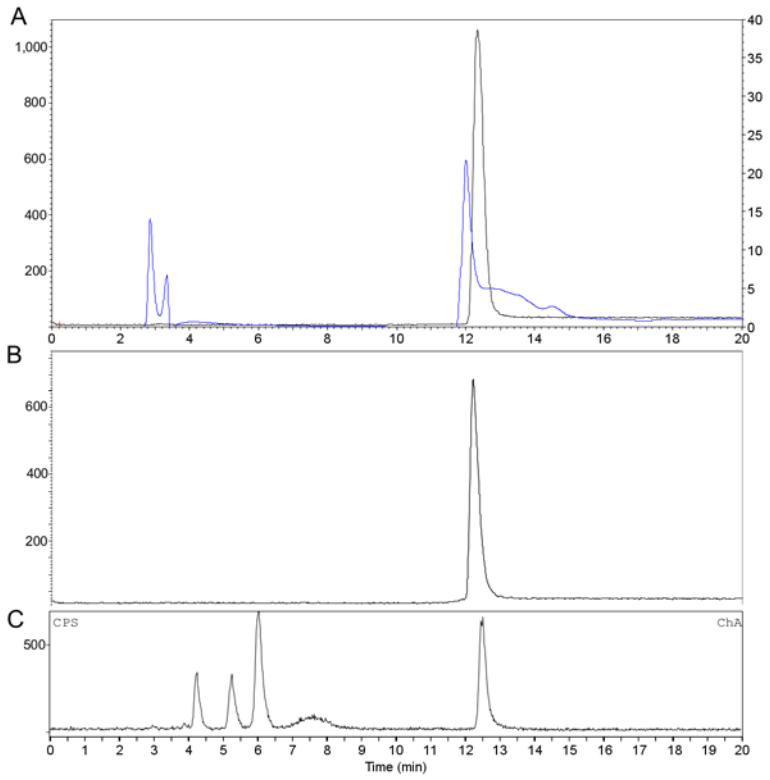

Figure 2: RP-HPLC analysis of purified [^{18}F]FB-anti-MMR 3.49 sdAb (A, γ-trace black, left axis, UV-trace blue, right axis t_R = 12.5 min) and after incubation for 3 hours in PBS pH 7.4 at room temperature (B, γ-trace). C: RP-chromatogram of urine obtained 30 minutes after injection of [^{18}F]FB-anti-MMR 3.49 (γ-trace).

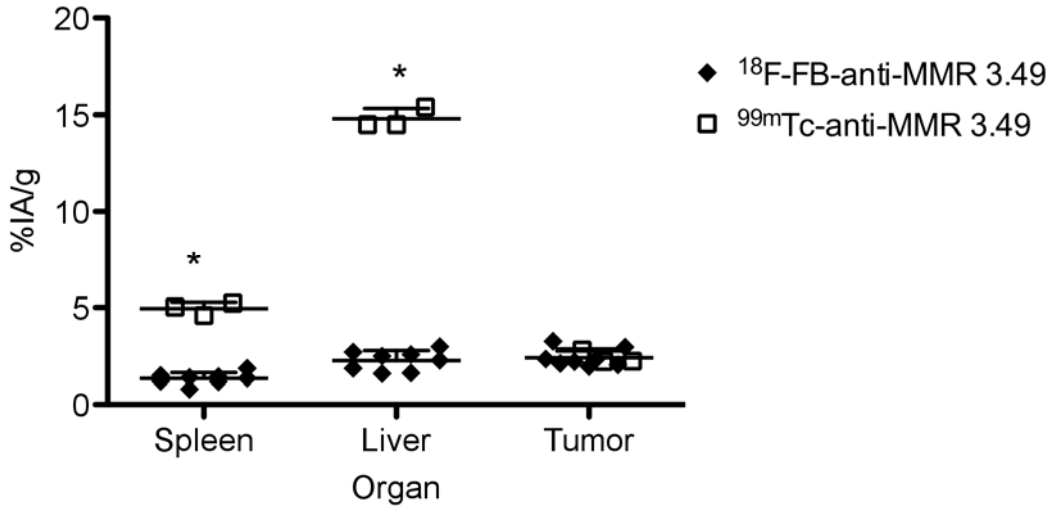

Figure 3: Comparison between uptake of [^{18}F]FB-anti-MMR 3.49 sdAb (◆) and ^{99m}Tc-anti-MMR 3.49 sdAb (□) in spleen, liver and tumor 3h pi. *Data is significantly different $p < 0.05$.

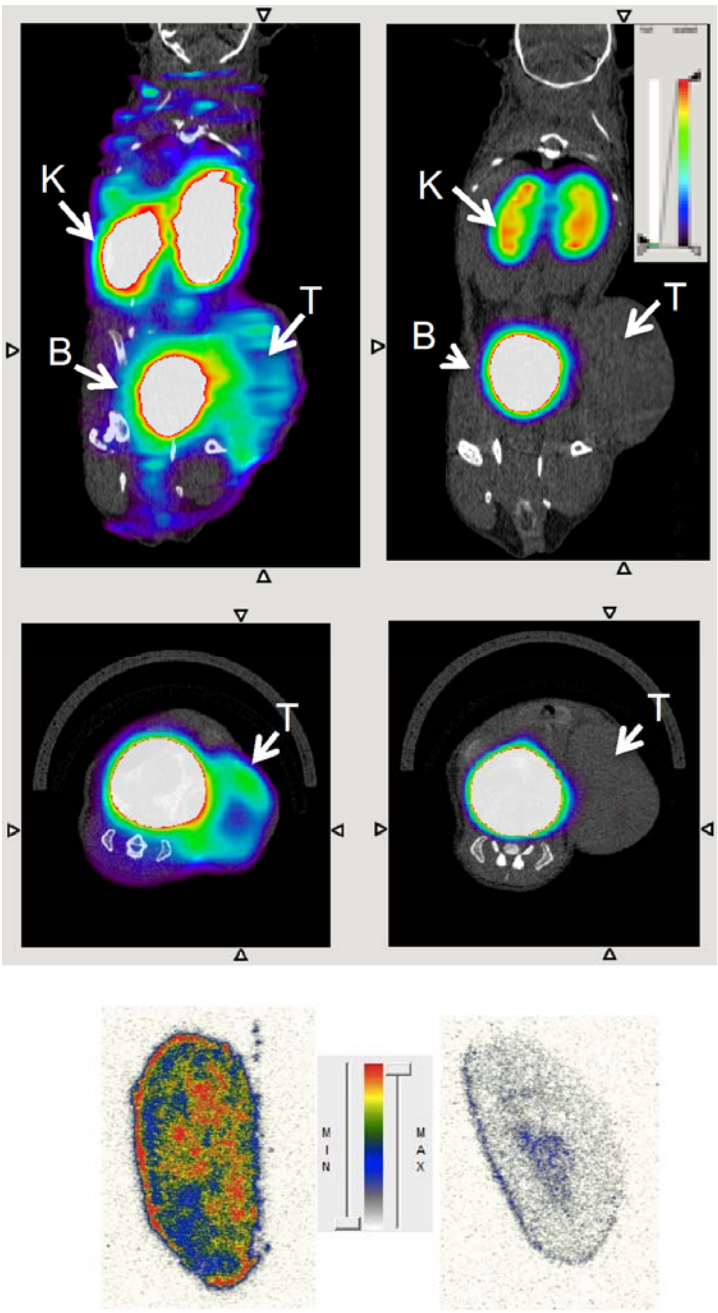

Figure 4: Transverse and coronal PET/CT images of WT (left) versus MMR deficient (right) 3LL-R tumor bearing mice scanned 3h p.i. of [^{18}F]FB-anti MMR 3.49. PET signals are encoded in color scale, CT-image in grey scale. Arrows point at tumor (T), kidney (K) and bladder (B). Autoradiography performed on slices from 3LL-R tumors grown in WT (left) versus MMR deficient (right) mice.

Table 1: Binding kinetics of sdAbs on human (h) and mouse (m) MMR.

	hMMR			mMMR		
sdAb*	k_a (M^{-1} s^{-1})	k_d (s^{-1})	K_D (nM)	k_a (M^{-1} s^{-1})	k_d (s^{-1})	K_D (nM)
14.4	1.4×10^{5}	1.4×10^{-3}	10	3.3×10^{4}	2.3×10^{-3}	68
5.38	2.0×10^{5}	6.6×10^{-4}	3.3	1.3×10^{5}	3.3×10^{-3}	25
26.7	5.8×10^{5}	7.3×10^{-3}	13	6.9×10^{5}	1.3×10^{-3}	1.9
3.49	4.4×10^{5}	8.0×10^{-4}	1.8	2.9×10^{5}	3.6×10^{-3}	12

Table 2: Biodistribution of ^{99m}Tc-anti-MMR sdAbs in 3LL-R-bearing WT and MMR-KO mice

Organ/Tissue	^{99m}Tc-anti-MMR 3.49 WT (n=3)	^{99m}Tc-anti-MMR 14.4 WT (n=3)	^{99m}Tc-anti-MMR 3.49 MMR-KO (n=2)
Heart	2.18 ± 0.15	2.77 ± 0.77	0.14 ± 0.02
Lungs	1.44 ± 0.15	0.92 ± 0.28	0.40 ± 0.08
Liver	14.79 ± 0.52	27.37 ± 3.37	0.61 ± 0.05
Spleen	4.94 ± 0.32	6.20 ± 1.69	0.22 ± 0.04
Kidney	146.61 ± 2.85	69.30 ± 11.46	234.77 ± 25.91
Muscle	0.57 ± 0.14	0.42 ± 0.11	0.06 ± 0.02
Bone	1.88 ± 0.17	1.78 ± 0.81	0.12 ± 0.01
Lymph nodes	3.04 ± 0.33	3.02 ± 0.46	0.19 ± 0.04
Blood	0.30 ± 0.03	0.13 ± 0.02	0.18 ± 0.03
Tumor	2.41 ± 0.34	1.40 ± 0.26	ND

Data are obtained 3h p.i. and expressed as mean %IA/g ± SD.

Table 3: Biodistribution of [^{18}F]FB-anti-MMR 3.49 sdAb in 3LL-R bearing WT, MMR-deficient and CCR-2 deficient mice at 3h p.i.

Organ/Tissue	WT mice (n=8)	MMR-KO mice (n=8)	CCR2-KO mice (n=5)
Lungs	1.60 ± 0.40	0.82 ± 0.52	1.45 ± 0.14
Heart	0.81 ± 0.11	0.28 ± 0.12*	1.00 ± 0.14
Liver	2.26 ± 0.51	0.52 ± 0.30*	2.54 ± 0.31
Spleen	1.34 ± 0.31	0.38 ± 0.16*	1.71 ± 0.69
Kidney	7.98 ± 0.86	4.76 ± 2.76	7.60 ± 0.76
Muscle	0.37 ± 0.14	0.10 ± 0.07*	0.42 ± 0.27
Bone	0.67 ± 0.28	0.15 ± 0.02*	1.03 ± 0.20
Blood	1.02 ± 0.31	0.73 ± 0.31	1.16 ± 0.20
Tumor	2.40 ± 0.46	0.29 ± 0.14*	1.42 ± 0.17†

Data are expressed as mean %IA/g ± SD

*† data is significantly different $p < 0.05$